

Bilayered semiconductor graphene nanostructures with periodically arranged hexagonal holes

Dmitry G. Kvashnin¹ (✉), Péter Vancsó², Liubov Yu. Antipina³, Géza I. Márk², László P. Biró², Pavel B. Sorokin^{1,3}, and Leonid A. Chernozatonskii¹ (✉)

¹ Emanuel Institute of Biochemical Physics, 4 Kosigina Street, Moscow, 119334, Russia

² Institute of Technical Physics and Materials Science, Research Centre for Natural Sciences, H-1525 Budapest, P.O. Box 49, Hungary

³ Technological Institute of Superhard and Novel Carbon Materials, 7a Centralnaya Street, Troitsk, Moscow, 142190, Russia

Received: 18 July 2014

Revised: 10 September 2014

Accepted: 13 October 2014

© Tsinghua University Press
and Springer-Verlag Berlin
Heidelberg 2014

KEYWORDS

graphene,
antidots,
electronic properties,
DFT

ABSTRACT

We present a theoretical study of new nanostructures based on bilayered graphene with periodically arranged hexagonal holes (bilayered graphene antidots). Our *ab initio* calculations show that fabrication of hexagonal holes in bigraphene leads to connection of the neighboring edges of the two graphene layers with formation of a hollow carbon nanostructure sheet which displays a wide range of electronic properties (from semiconductor to metallic), depending on the size of the holes and the distance between them. The results were additionally supported by wave packet dynamical transport calculations based on the numerical solution of the time-dependent Schrödinger equation.

1 Introduction

Graphene, a two-dimensional (2D) carbon crystal with honeycomb structure was first isolated by the micromechanical cleavage of graphite in 2004 [1, 2]. Beside the monolayer film, bilayered graphene attracts specific attention due to its particular electronic properties [3]. Like in the case of monolayers, the bilayered graphene is a semimetal, but its conduction and valence bands touch with quadratic dispersion, unlike the linear dispersion relation seen in monolayer graphene [4]. Therefore, the problem of the lack of a

semiconductor band gap remains in bilayered graphene. The fabrication of bilayered graphene ribbons or adsorption of adatoms to the bilayered graphene structure, like in the case of single-layer graphene [5–7], can open a band gap, but also create scattering regions whereas it is highly desirable to avoid the depression of mobility of the π -electrons. It is possible to open a gap using an electric field effect, [8] but its size is tiny, and cannot be used in semiconductor devices.

A promising way to open a band gap in graphene is the making of periodical nanopores in the structure. It was predicted that such periodic arrays of holes in

Address correspondence to Dmitry G. Kvashnin, dgkvashnin@gmail.com; Leonid A. Chernozatonskii, cherno@sky.chph.ras.ru

a graphene lattice would transform graphene from semimetal to semiconductor with a tunable band gap by changing the period and the size of the holes [9–11]. Periodic nanopores have been experimentally realized by different methods [12–16], with general confirmation of theoretical predictions [9, 10, 17–20]. The transport measurements show that such materials display an effective energy gap (~100 meV) and an ON–OFF ratio up to 10, which is a promising feature of the graphene antidot scheme [21, 22]. It can be speculated that while in the case of a graphene monolayer such holes act as scattering edges, in the case of a bilayered structure the neighboring graphene edges can connect with each other (as has been shown in several experimental papers on the formation of a closed-edge structure [23–26] after e-beam irradiation of the bilayered graphene). This creates a bilayer hollow graphene material without edges, i.e. without any interruption of the sp^2 carbon lattice. Such kind of structures with closed-edges can be described as a complex structure that combines the flat geometry of graphene with the curvature of small diameter nanotubes. Curvature effects induce local hybridization, which can bring new physics, generating new opportunities to apply bigraphene-based nanostructures in nanoelectronic devices. A further advantage may be that while the building of a regular carbon nanotube lattice from individual CNTs seems less feasible, a regular structure resembling such a lattice may be produced by the coupling of the atomic bonds at the edges of bilayered graphene antidot lattice.

Here we will show that creating holes in bilayered graphene leads to the formation of a family of novel closed-edge hollow nanostructures with special electronic properties. We found that the highly strained edges of the bilayered graphene holes tend to compensate dangling bonds by the stitching of the edges of the two layers. We investigated the electronic properties of these superlattices with hexagonal unit cells and found that depending upon the atomic geometry (the size of the holes and the distance between them) both semiconducting (with band gap ~1 eV) and metallic behavior can occur. The propagation of the electrons was also studied using a wave packet dynamics (WPD) transport approach.

The organization of the paper is as follows. In

Sec. 2 the calculation methods are presented. Section 3 consists of three parts. The first part gives the results of the investigation of the stability and formation of bilayered graphene superlattices (BGS) with connected layers and hexagonal holes. In the second part of Section 3 the investigation of the electronic properties depending on the geometric parameters was performed and the origin of the specific electronic properties was discussed. The third part is devoted to the calculation of the transport properties. Section 4 contains the discussion of the results.

2 Calculation methods

The investigation of the geometry and stability of the BGS were made from an energetic point of view using density functional theory with the local density approximation (DFT-LDA) implemented in the SIESTA package with periodic boundary conditions [27]. To calculate equilibrium atomic structures, the Brillouin zone was sampled according to the Monkhorst–Pack [28] scheme with a k -point density of 0.08 \AA^{-1} . In the course of the atomic structure minimization, structural relaxation was carried out until the change in the total energy was less than 10^{-4} eV , or forces acting on each atom were less than 10^{-3} eV/\AA . The number of atoms in the hexagonal unit cell was 150 to 1,000, depending on the structural parameters.

The electronic properties were calculated using the DFTB approach [29], with a second-order expansion of the Kohn–Sham total energy in density functional theory with respect to charge density fluctuations implemented in DFTB+ software package. This method can provide qualitative data about the changes of the value of the band gap. DFTB is a well-established way to describe the complex properties of materials [29]. The band structures were constructed with sets of k -points from 5 to 20 depending on the size of the unit cell in each of the high-symmetry directions.

We performed transport calculations of the modelled BGS by using WPD [30], which is able to handle systems containing a larger number of C atoms than *ab initio* calculations. A further advantage of the WPD method is that it makes it possible to identify the scattering sites responsible [31] for the characteristic features of transport functions.

In our geometry, the wave packet (WP) is injected from a metallic electrode to the semi-infinite structure modeling a transport measurement setup. The metallic electrode is approximated by a jellium potential with Fermi energy $E_F = 5$ eV and work function $W = 4.81$ eV. For the considered BGS, we used a local one-electron pseudopotential [32] matching the band structure of graphite and graphene sheet. This parameterized potential $V(\mathbf{r}) = \sum_{j=1}^N \sum_{i=1}^3 A_i e^{-a_i |\mathbf{r}-\mathbf{r}_j|^2}$, where \mathbf{r}_j denotes the atomic positions and N is the number of the atoms, has also been successfully applied for carbon nanotubes [33] and graphene grain boundaries [34]. The incoming wave packet from the electrode was launched with $E_k = E_F = 5$ eV kinetic energy and had a spatial width of $\Delta y = 0.37$ nm, $\Delta x = \Delta z = \infty$. The time development of the wave packets were calculated using a modified version of our computer code developed for solving the time-dependent Schrödinger equation for carbon nanotubes and graphene [35, 36].

3 Results and discussion

Here we consider BGS in which the hexagonal holes have zigzag edges. Such a type of edges was chosen based on experimental data [13, 37] where holes with predominantly zigzag edges were obtained after graphene etching. Moreover, according to theoretical predictions, armchair edges of bilayered graphene cannot form a closed structure due to geometrical incompatibility [26]. Due to the high in-plane elastic constant and small bending modulus, graphene tends to minimize edge energy by out of plane bending (if it can). This effect is responsible for the bending of narrow graphene nanoribbons with bare edges [23, 38]. Whereas in the case of a graphene monolayer the edges predominantly display an in-plane reconstruction, the presence of the highly strained edges of the neighboring layers in BGS leads to the bending and connection of the two edges to compensate for dangling bonds (the same behavior was observed in bigraphene edges, see Refs. [24–26]). Therefore, the creation of the periodically arranged holes in bigraphene should lead to fabrication of hollow carbon structures with closed edges, as illustrated in Figs. 1(a) and 1(b). We

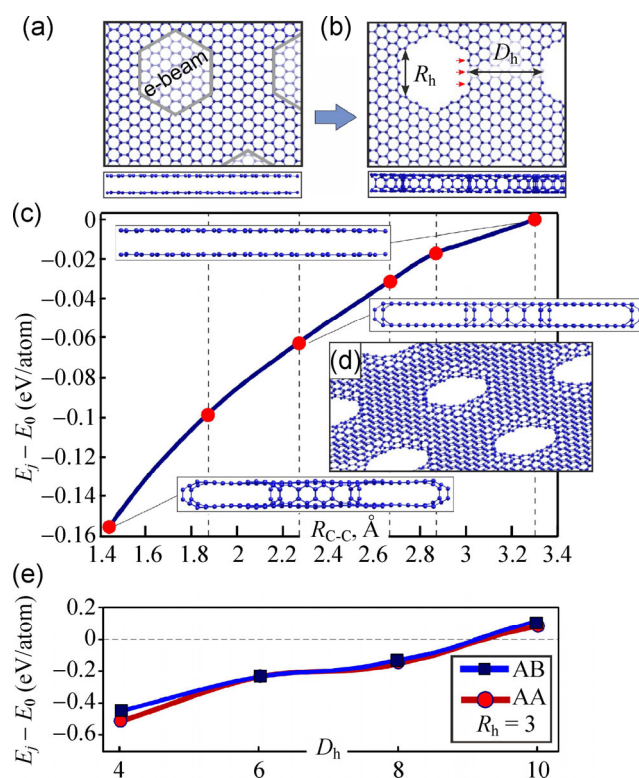


Figure 1 The proposed fabrication scheme. (a) Top and side view of the pristine structure of bilayered graphene in “AA” stacking with the depicted area for holes and (b) such a structure with created holes. The red arrows denote the atoms on the top layer that connect with the atoms on the bottom layer. In the lower figure the atomic connections are visible. R_h and D_h are the two geometrical parameters which define the structure, see the text for details. (c) Energy barrier calculated for the (3, 8) structure versus the distance between edges of two graphene layers. E_0 denotes the energy of the initial structure. In the inset (d) the 3D view of the (3, 8) BGS is presented. (e) Relative energy between initial (edges are not connected) and final (edges are connected) states of BGS structures with various values of D_h .

found that such a process occurs without any activation barrier (Fig. 1(c)) for any of the structures considered in this work, and therefore we can expect that during an experiment such a structure will be formed spontaneously.

The properties of BGS are directly related to the atomic geometry or more specifically to the size of the holes and the distance between them as well as the flattening of the region between the holes [25]. With increasing hole size the whole structure tends to the geometry of a carbon nanotube network, which can display semiconducting properties [39, 40], whereas with increasing distance between the holes the

geometry of the structure tends to that of the semimetallic bilayered graphene. According to these facts we classify BGS structures using two independent parameters: size of the holes R_h (the length of one edge of the hexagonal hole in the units of graphene unit cell in the zigzag direction) and distance between holes D_h (in the units of graphene unit cell in the armchair direction) (Fig. 1(b)).

Figure 1(c) shows the “relative energy” (energy difference between the transition and initial structures) as a function of the distance between the atoms on the adjacent edges in the two layers for a particular parameter pair ($R_h = 3$, $D_h = 8$). By decreasing the distance between the atoms on the adjacent edges of the holes, the relative energy decreases and tends to the minimum value (~ -0.16 eV/atom). The minimum of the relative energy corresponds to a structure with a bond length between the carbon atoms from neighboring layers equal to 1.415 Å. Such value of the bond length matches well with the equilibrium bond length between sp^2 carbon atoms. Further decreasing the distance leads to a sharp increase in energy. This fact allows us to conclude that in the absence of impurities on the edges of the holes the connected layers (BGS) form a stable configuration.

It should be noted that the spontaneous formation occurs not only for the “AA” stacked bigraphene (which is less favorable in energy) but also for the more favorable Bernal stacked BGS. Bernal stacked bilayered graphene with periodically arranged holes without connections between the layers means that the holes were made in “AA” stacked graphene and then the layers were shifted. Only in the case when the distance between the holes was larger than the size of the holes does the connection between the layers take place after the stacking transformation from “AB” to “AA” by means of the shifting of the layers relative to each other with further formation of bonds between the layers.

With increasing R_h the regions between the holes tend to become narrow zigzag graphene nanoribbons with edges of high chemical activity. This leads to the bending of the ribbon [38] with a further decrease of the distance between the layers and further formation of chemical bonds between them. In both stacking modes at a fixed D_h , due to the increasing of R_h (size

of the holes) the relative energy is negative in all the range of R_h which proves that the structures with connected layers (BGS) are the energetically preferable configurations.

Figure 1(e) shows the relative energy as a function of the second parameter D_h (distance between the holes). With increasing distance between the holes, the relative energy increases and becomes positive. In that case the nanoribbons between the holes become wider and can't minimize their energy due to bending, and hence they remain flat. During the geometry optimization, the structure remains bilayered graphene without a transformation from “AB” to “AA” stacking.

The pronounced dependence of the shape of the BGS upon the R_h and D_h parameters allows us to predict drastically different behavior of the electronic properties for the different structures. Indeed, we found that the variation of the parameters allows us to tune the conductivity from semiconducting to metallic. In order to explore this variation, we consider the electronic properties for a wide range of the structural parameters with the total number of atoms in unit cell varying from 150 to 1,500.

In Figs. 2(a) and 2(b), the dependence of the band gap on the D_h parameter for structures with fixed R_h values of 2 and 3, respectively, are presented. We found that in both cases the band gap decreases with the increase of the distance between the holes (D_h), according to a quantum confinement law $E_{\text{gap}} \sim a_0 \frac{1}{(D_h)^n}$ (where a_0 and n are fitting coefficients).

At the infinite limit of D_h , the electronic structure tends to the bilayered graphene with zero band gap. For values of R_h of 2 and 3, the fitting coefficients were obtained as $a_0 = 0.43$, $n = 1.41$ (Fig. 2(a)) and $a_0 = 0.11$, $n = 1.81$ (Fig. 2(b)), respectively. In the case of the variation of R_h (size of the holes) at fixed D_h (Fig. 2(c)) the behavior of the band gap displays a more complex character. It shows a decrease of the band gap according to the quantum confinement law $E_{\text{gap}} \sim a_1 \frac{1}{(R_h)^n}$ (where a_1 and n are the fitting coefficients). The slight oscillations can be attributed to the complex geometry of the structure (the presence of nanotube Y-junctions which contain topological defects represented by eight-membered carbon rings)

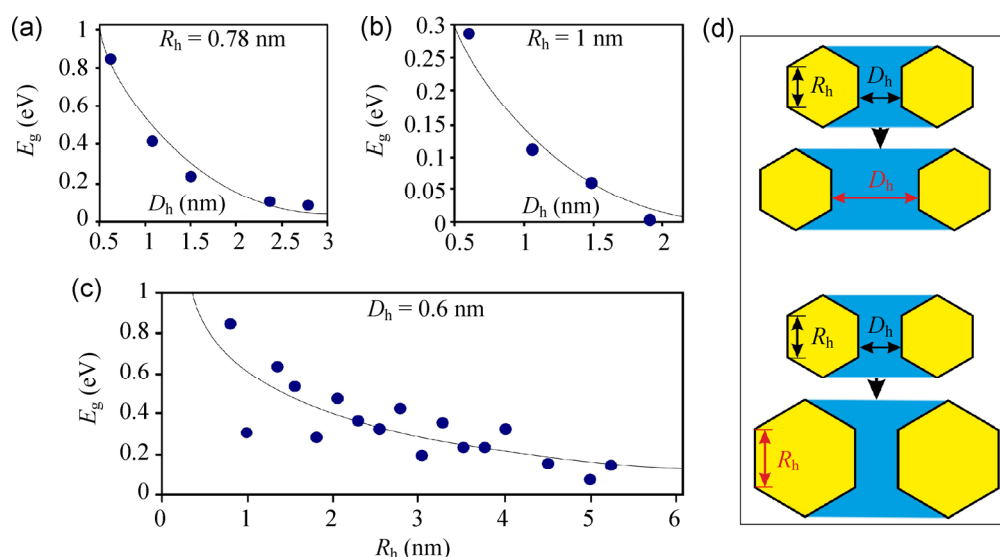


Figure 2 The dependence of the band gap on the two main parameters: (a) and (b) D_h , the distance between the holes and (c) R_h , the hole size. (d) Changing of the main parameters for (a), (b) and (c).

which strongly affects the electron distribution and the electronic properties of BGS. Obtained values of the fitting coefficients are $a_1 = 0.67$, $n = 0.76$.

It is important to notice that Fig. 2 shows the asymptotic limits of the two main parameters. In both cases the band gap tends to zero, because asymptotic limits of D_h and R_h correspond to geometries of metallic bilayered graphene and metallic armchair carbon nanotube (CNT), respectively. Note that in earlier reports [41, 42] bilayered graphene superlattices with rectangular unit cells were studied. All the considered structures display semimetal properties apart from the noncovalently bonded bilayered nanomesh [42].

It should be noted, however, that not only the structures with high values of R_h can have low values of the band gap. Decreasing the size of the holes to become point defects (vacancies) leads to an appearance of metallic properties without any dependence on the distance between the vacancies. This peculiar behavior of the band gap does not follow the dependence presented in Fig. 2(c), because point defects are not included in our classification. In our classification a BGS is described by means of the length of the edge of hexagonal holes in the zigzag direction, but the point defects cannot be described as hexagonal holes. This particular case, the unit cell of the bilayered

graphene with point defects, is presented in Fig. 3(a). Figure 3(b) shows the metallic band structure and the corresponding partial electron density of states (colored lines), as well as the total DOS (black line). The appearance of metallicity originates from the intermediate hybridization state of the carbon atoms: the high curvature of the carbon lattice leads to a transition of the electronic states of the atoms marked by purple from the sp^2 to sp^3 state, but the absence of the fourth neighbor for them creates a dangling bond with unsaturated conduction electrons. From Figs. 3(a) and 3(b), we can observe that the metallic behavior mainly originates from the atoms marked in purple (first neighbor atoms).

In order to investigate not only the electronic, but also the transport properties of the modeled BGS, we performed WPD calculations. Two specific BGS with semiconductor and metallic properties were selected. Figure 4 shows the model geometry, together with three snapshots from the time evolution of the probability density $\rho(r, t)$, for the case of the semiconducting BGS. These 2D (XY) images illustrate the charge spreading on the top layer of the BGS. In the first frame at $t = 0.2$ fs the WP coming from the y direction (denoted by red arrows in Fig. 4(a)) is still in the jellium electrode. At $t = 3$ fs a part of the WP has already penetrated about 2 nm into the BGS, while a

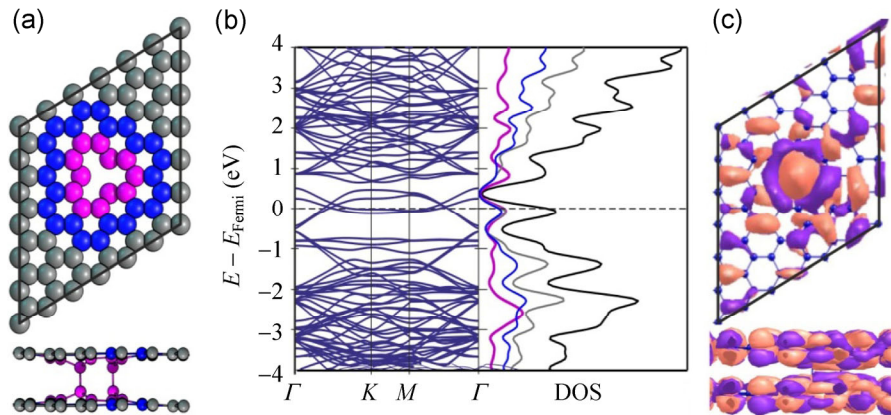


Figure 3 BGS with point defects: (a) atomic structure of the unit cell of BGS with point defects (top and side view); (b) band structure and density of states. Different colors show partial densities of states at the different atoms; (c) the wave function distribution at the Fermi level with isovalue 0.03 electrons per cubic angstrom (top and side view, the two colors denote the positive and negative signs of the wave function).

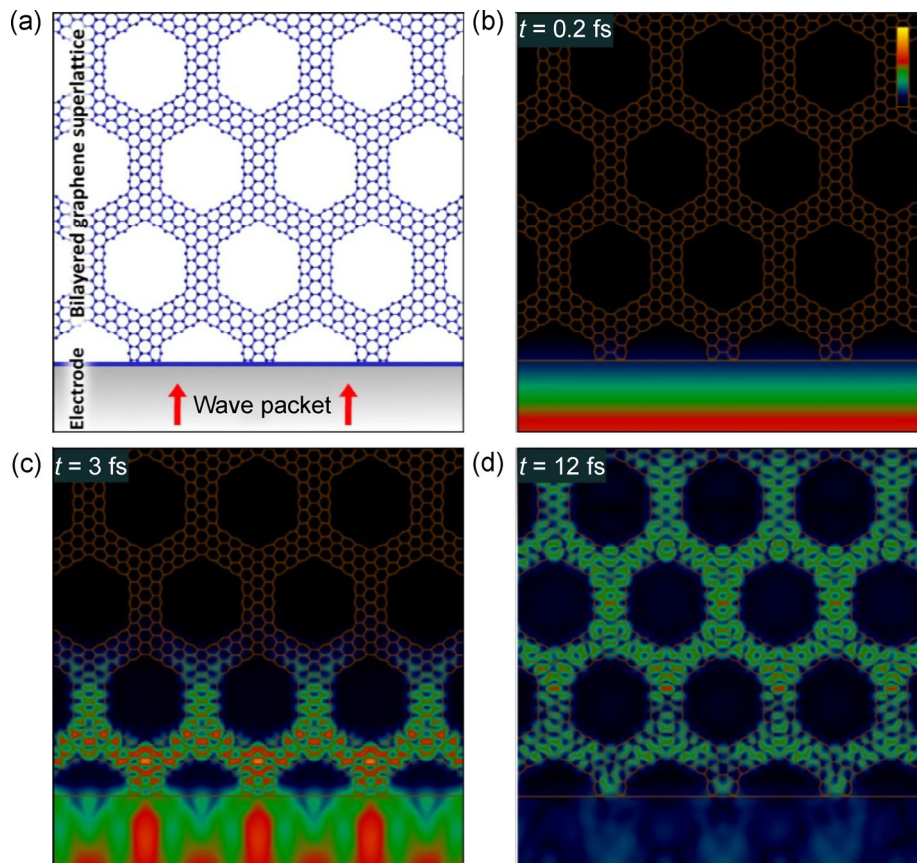


Figure 4 (a) Top view of the model geometry of the metallic electrode and the semi-infinite semiconducting BGS. (b)–(d) Selected snapshots from the time evolution of the probability density of the wave packet shown as color-coded 2D (top view XY) sections. Black corresponds to zero, yellow to the maximum density (9.78×10^{-5}) [see the scale bar in (b)]. The size of the presentation window is 7.68 nm.

part of it is reflected back to the jellium electrode. By $t = 12$ fs the electrode has become empty and the WP spreads over the whole BGS surface. Due to the finite energy spread of the initial WP, different energies are mixed in the snapshots of the time evolution (Fig. 4).

In order to study the dynamics at well defined energy values, we performed a time-energy ($t \rightarrow E$) Fourier transform, and thus we calculated $\psi(\mathbf{r}, E)$ from $\psi(\mathbf{r}, t)$. The probability current $I(\mathbf{r}, E)$ and the transmission function $T(E)$ is calculated from $\psi(\mathbf{r}, E)$ [34]. Figure 5 shows the probability density distributions and the corresponding transmission functions at the Fermi energy for the semiconductor and metallic BGS. In the semiconductor case the probability density shows a decay in the BGS (Fig. 5(a)), and no further spreading occurs at the Fermi energy, opening a 0.6 eV transport gap. In contrast, the WP spreads along the whole metallic BGS with a high transmission probability.

The effect of the (CNT) Y-junctions on the electronic transport can be also seen in Fig. 5(b). The atomic structure of such a kind of CNT Y-junctions were

considered in Ref. [43] and called “planar jungle gyms”. The slightly decreased probability density at the junctions corresponds to the reduced DOS at the Fermi energy calculated by DFT.

4 Conclusions

We have studied in detail novel hexagonal nanomeshes based on bilayered graphene. The atomic structure and the formation process were investigated using density functional theory. It was found that after making holes in the bilayered graphene lattice, the two layers tend to connect with each other along the edges of the holes without any activation barrier (in the absence of impurity atoms in the edges). Using the DFTB approximation, the electronic properties of the BGS and the dependence of the band gap on the two main parameters characterizing the geometry were studied in detail. In the asymptotic case, for both parameters the band gap tends to zero. A special case of the metallic BGS with point defects was also considered. Electron transport through different BGS

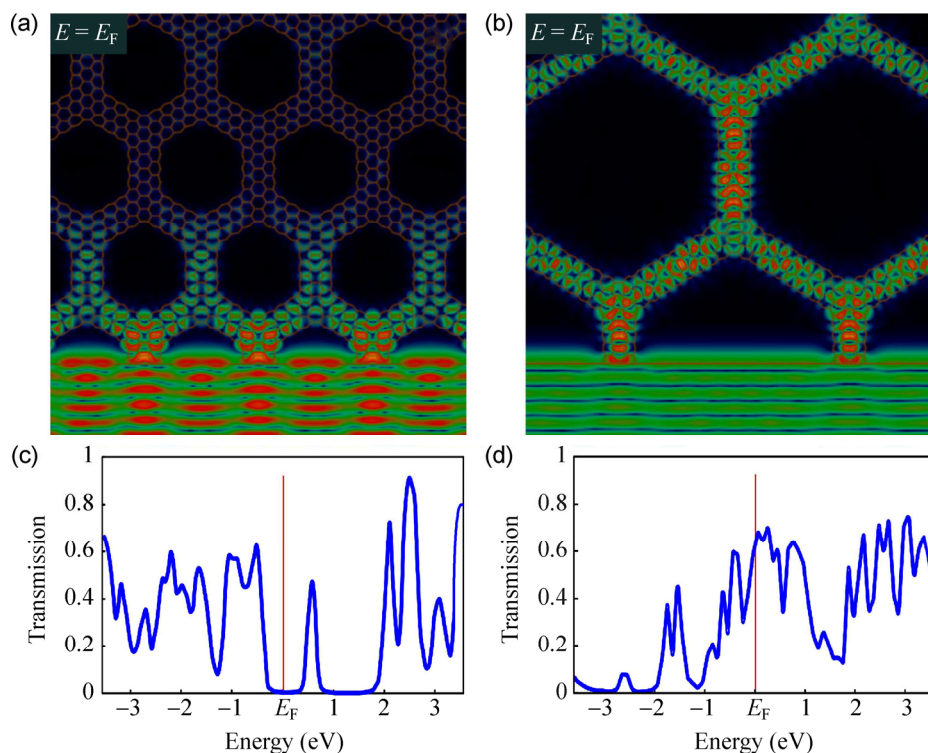


Figure 5 (a) and (b) Probability density on the semiconductor and metallic BGS at the Fermi energy shown by color-coded 2D (top view XY) sections. The images are renormalized individually to their maximum density. The maximum density values are 5.23×10^{-5} and 1.31×10^{-4} for (a) and (b), respectively; (c) and (d) Transmission functions of the two BGS.

was calculated by the wave packet dynamics method. The results confirm the semiconductor and metallic properties. The presented results can serve as a basis for the further investigation and fabrication of jointless (absence of stacking faults) hollow semiconducting materials with tunable electronic properties, with potential applications in mobility nanoelectronic devices.

Acknowledgements

This work was supported by an EU Marie Curie International Research Staff Exchange Scheme Fellowship within the 7th European Community Framework Programme (MC-IRSES proposal 318617 FAEMCAR project) OTKA 101599 in Hungary. We are grateful to the Joint Supercomputer Center of the Russian Academy of Sciences and “Lomonosov” research computing center for the possibilities of using a cluster computer for the quantum-chemical calculations. D.G.K. acknowledges the support from the Russian Ministry of Education and Science (No. 948 from 21 of November 2012).

References

- [1] Novoselov, K. S.; Geim, A. K.; Morozov, S. V.; Jiang D.; Zhang Y.; Dubonos, S. V.; Grigorieva, I. V.; Firsov, A. A. Electric field effect in atomically thin carbon films. *Science* **2004**, *306*, 666–669.
- [2] Novoselov, K. S.; Jiang, D.; Schedin, F.; Booth, T. J.; Khotkevich, V. V.; Morozov, S. V.; Geim, A. K. Two-dimensional atomic crystals. *Proc. Natl. Acad. Sci. USA* **2005**, *102*, 10451–10453.
- [3] McCann, E.; Koshino, M. The electronic properties of bilayer graphene. *Rep. Prog. Phys.* **2013**, *76*, 056503.
- [4] McCann, E.; Fal’ko, V. I. Landau-level degeneracy and quantum hall effect in a graphite bilayer. *Phys. Rev. Lett.* **2006**, *96*, 086805.
- [5] Chernozatonskii, L. A.; Sorokin, P. B.; Brüning, J. W. Two-dimensional semiconducting nanostructures based on single graphenesheets with lines of adsorbed hydrogen atoms. *Appl. Phys. Lett.* **2007**, *91*, 183103.
- [6] Chernozatonskii, L. A.; Sorokin, P. B.; Belova, E. É.; Brüning, J.; Fedorov, A. S. Superlattices consisting of “lines” of adsorbed hydrogen atom pairs on graphene. *JETP Lett.* **2007**, *85*, 77–81.
- [7] Chernozatonskii, L. A.; Sorokin, P. B. Nanoengineering-structures on graphenewith adsorbed hydrogen “lines”. *J. Phys. Chem. C* **2010**, *114*, 3225–3229.
- [8] Castro, E. V.; Novoselov, K. S.; Morozov, S. V.; Peres, N. M. R.; Lopes dos Santos, J. M. B.; Nilsson, J.; Guinea, F.; Geim, A. K.; Castro Neto, A. H. Biased bilayer graphene: Semiconductor with a gap tunable by the electric field effect. *Phys. Rev. Lett.* **2007**, *99*, 216802.
- [9] Liu, X. F.; Zhang, Z. H.; Guo, W. L. Universal rule on chirality-dependent bandgapsin grapheneantidotlattices. *Small* **2013**, *9*, 1405–1410.
- [10] Pedersen, T. G.; Flindt, C.; Pedersen, J.; Jauho, A.-P.; Mortensen, N. A.; Pedersen, K. Optical properties of grapheneantidotlattices. *Phys. Rev. B* **2008**, *77*, 243431.
- [11] McCann, E. Asymmetry gap in the electronic band structure of bilayer graphene. *Phys. Rev. B* **2006**, *74*, 161403.
- [12] Nemes-Incze, P.; Magda, G.; Kamarás, K.; Biró, L. P. Crystallographicallyselective nanopatterningof grapheneon SiO₂. *Nano Res.* **2010**, *3*, 110–116.
- [13] Dobrik, G.; Nemes-Incze, P.; Tapasztó, L.; Lambin, P.; Biró, L. P. Nanoscalelithography of graphenewith crystallographic orientation control. *Physica E* **2012**, *44*, 971-975.
- [14] Lee, J.-H.; Jang, Y.; Heo, K.; Lee, J.-M.; Choi, S. H.; Joo, W.-J.; Hwang, S. W.; Whang, D. Large-scale fabrication of 2D nanoporousgrapheneusing a thin anodic aluminum oxide etching mask. *J. Nanosci.Nanotechnol.* **2013**, *13*, 7401–7405.
- [15] Zubeltzu, J.; Chuvilin, A.; Corsetti, F.; Zurutuza, A.; Artacho, E. Knock-on damage in bilayer graphene: Indications for a catalytic pathway. *Phys. Rev. B* **2013**, *88*, 245407.
- [16] Bai, J. W.; Zhong, X.; Jiang, S.; Huang, Y.; Duan, X. F. Graphenenanomesh. *Nat. Nanotechnol.* **2010**, *5*, 190–194.
- [17] Dvorak, M.; Oswald, W.; Wu, Z. G. Bandgapopening by patterning graphene. *Sci. Rep.* **2013**, *3*, 2289.
- [18] Pedersen, T. G.; Flindt, C.; Pedersen, J.; Mortensen, N. A.; Jauho, A.-P.; Pedersen, K. Grapheneantidotlattices: Designed defects and spin qubits. *Phys. Rev. Lett.* **2008**, *100*, 136804.
- [19] Ouyang, F. P.; Peng, S. L.; Liu, Z. F.; Liu, Z. R. Bandgapopening in grapheneantidotlattices: The missing half. *ACS Nano* **2011**, *5*, 4023–4030.
- [20] Fürst, J. A.; Pedersen, J. G.; Flindt, C.; Mortensen, N. A.; Brandbyge, M.; Pedersen, T. G.; Jauho, A.-P. Electronic properties of grapheneantidotlattices. *New J. Phys.* **2009**, *11*, 095020.
- [21] Sinitetskii, A.; Tour, J. M. Patterning graphenethrough the self-assembled templates: Toward periodic two-dimensional graphenenanostructures with semiconductor properties. *J. Am. Chem. Soc.* **2010**, *132*, 14730–14732.
- [22] Kim, M.; Safron, N. S.; Han, E.; Arnold, M. S.; Gopalan, P. Fabrication and characterization of large-area, semiconducting

- nanoperforatedgraphenematerials. *Nano Lett.* **2010**, *10*, 1125–1131.
- [23] Liu, Z.; Suenaga, K.; Harris, P. J. F.; Iijima, S. Open and closed edges of graphenelayers. *Phys. Rev. Lett.* **2009**, *102*, 015501.
- [24] Campos-Delgado, J.; Kim, Y. A.; Hayashi, T.; Morelos-Gómez, A.; Hofmann, M.; Muramatsu, H.; Endo, M.; Terrones, H.; Shull, R. D.; Dresselhaus, M. S.; et al. Thermal stability studies of CVD-grown graphenenanoribbons: Defect annealing and loop formation. *Chem.Phys.Lett.* **2009**, *469*, 177–182.
- [25] Algara-Siller, G.; Santana, A.; Onions, R.; Suyetin, M.; Biskupek, J.; Bichoutskaia, E.; Kaiser, U. Electron-beam engineering of single-walled carbon nanotubes from bilayer graphene. *Carbon* **2013**, *65*, 80–86.
- [26] Zhan, D.; Liu, L.; Xu, Y. N.; Ni, Z. H.; Yan, J. X.; Zhao, C.; Shen, Z. X. Low temperature edge dynamics of AB-stacked bilayer graphene: Naturally favored closed zigzag edges. *Sci. Rep.* **2011**, *1*, 12.
- [27] Soler, J. M.; Artacho, E.; Gale, J. D.; García, A.; Junquera, J.; Ordejón, P.; Sánchez-Portal, D. The siesta method for abinitioorder-Nmaterials simulation. *J. Phys.: Condens. Mat.* **2002**, *14*, 2745–2779.
- [28] Monkhorst, H. J.; Pack, J. D. Special points for Brillouin-zone integrations. *Phys. Rev. B* **1976**, *13*, 5188–5192.
- [29] Elstner, M.; Porezag, D.; Jungnickel, G.; Elsner, J.; Haugk, M.; Frauenheim, T.; Suhai, S.; Seifert, G. Self-consistent-charge density-functional tight-binding method for simulations of complex materials properties. *Phys. Rev. B* **1998**, *58*, 7260–7268.
- [30] Garraway, B. M.; Suominen, K.-A. Wave-packet dynamics: New physics and chemistry in femto-time. *Rep. Prog. Phys.* **1995**, *58*, 365–419.
- [31] Vancsó, P.; Márk, G. I.; Lambin, P.; Mayer, A.; Hwang, C.; Biró, L. P. Effect of the disorder in graphenegrain boundaries: A wave packet dynamics study. *Appl. Surf. Sci.* **2014**, *291*, 58–63.
- [32] Mayer, A. Band structure and transport properties of carbon nanotubes using a local pseudopotential and a transfer-matrix technique. *Carbon* **2004**, *42*, 2057–2066.
- [33] Mayer, A. Transfer-matrix simulations of electronic transport in single-wall and multi-wall carbon nanotubes. *Carbon* **2005**, *43*, 717–726.
- [34] Vancsó, P.; Márk, G. I.; Lambin, P.; Mayer, A.; Kim, Y. S.; Hwang, C.; Biró, L. P. Electronic transport through ordered and disordered graphenegrain boundaries. *Carbon* **2013**, *64*, 101–110.
- [35] Márk, G. I.; Biró, L. P.; Gyulai, J. Simulation of STM images of three-dimensional surfaces and comparison with experimental data: Carbon nanotubes. *Phys. Rev. B* **1998**, *58*, 12645–12648.
- [36] Márk, G. I.; Vancsó, P.; Hwang, C.; Lambin, P.; Biró, L. P. Anisotropic dynamics of charge carriers in graphene. *Phys. Rev. B* **2012**, *85*, 125443.
- [37] Scuracchio, P.; Dobry, A. Bending mode fluctuations and structural stability of graphenenanoribbons. *Phys. Rev. B* **2013**, *87*, 165411.
- [38] Kit, O. O.; Tallinen, T.; Mahadevan, L.; Timonen, J.; Koskinen, P. Twisting graphenenanoribbons into carbon nanotubes. *Phys. Rev. B* **2012**, *85*, 085428.
- [39] Bekyarova, E.; Itkis, M. E.; Cabrera, N.; Zhao, B.; Yu, A. P.; Gao, J. B.; Haddon, R. C. Electronic properties of single-walled carbon nanotube networks. *J. Am. Chem. Soc.* **2005**, *127*, 5990–5995.
- [40] Timmermans, M. Y.; Estrada, D.; Nasibulin, A. G.; Wood, J. D.; Behnam, A.; Sun, D.-M.; Ohno, Y.; Lyding, J. W.; Hassanien, A.; Pop, E.; et al. Effect of carbon nanotube network morphology on thin film transistor performance. *Nano Res.* **2012**, *5*, 307–319.
- [41] Chernozatonskii, L. A.; Demin, V. A. Nanotube connections in bilayer graphene with elongated holes. In *Proceedings of the International Conference in Nanomaterials: Applications and Properties*, Alushta, the Crimea, 2013, pp. 03NCNN32–03NCNN34.
- [42] Chernozatonskii, L. A.; Demin, V. A.; Artyukh, A. A. Bigraphenenanomeses: Structure, properties, and formation. *JETP Lett.* **2014**, *99*, 309–314.
- [43] Chernozatonskii, L. A. Carbon nanotube connectors and planar jungle gyms. *Phys. Lett. A* **1992**, *172*, 173–176.